ELSEVIER

Journal of Contaminant Hydrology 37 (1999) 269–293

JOURNAL OF
Contaminant
Hydrology

Biodegradation during contaminant transport in porous media: 1. mathematical analysis of controlling factors

Mark L. Brusseau [a,b,*], Lily H. Xie [b], Li Li [a]

[a] *Department of Soil, Water and Environmental Science, 429 Shantz Building, University of Arizona, 38 Tucson, AZ 85721, USA*

[b] *Department of Hydrology and Water Resources, 429 Shantz, University of Arizona, Tucson, AZ 85721, USA*

Received 29 April 1998; received in revised form 28 December 1998; accepted 28 December 1998

Abstract

Interest in coupled biodegradation and transport of organic contaminants has expanded greatly in the past several years. In a system in which biodegradation is coupled with solute transport, the magnitude and rate of biodegradation is influenced not only by properties of the microbial population and the substrate, but also by hydrodynamic properties (e.g., residence time, dispersivity). By nondimensionalizing the coupled-process equations for transport and nonlinear biodegradation, we show that transport behavior is controlled by three characteristic parameters: the effective maximum specific growth rate, the relative half-saturation constant, and the relative substrate-utilization coefficient. The impact on biodegradation and transport of these parameters, which constitute various combinations of factors reflecting the influences of biotic and hydraulic properties of the system, are examined numerically. A type-curve diagram based on the three characteristic parameters is constructed to illustrate the conditions under which steady and non-steady transport is observed, and the conditions for which the linear, first-order approximation is valid for representing biodegradation. The influence of constraints to microbial growth and substrate utilization on contaminant transport is also briefly discussed. Additionally, the impact of biodegradation, with and without biomass growth, on spatial solute distribution and moments is examined.

Keywords: Coupled biodegradation; Contaminant transport; Porous media

* Corresponding author. Fax: +1-602-621-1647; e-mail: brusseau@ag.arizona.edu

0169-7722/99/$ - see front matter
PII: S0169-7722(99)00005-4

1. Introduction

Interest in coupled biodegradation and transport of organic contaminants has expanded greatly in the past several years. Concomitantly, many models have been developed to simulate biodegradation and transport of contaminants in porous media. In the majority of these models, biodegradation is represented with either the first-order or Monod approach (Brusseau et al., 1992). Unfortunately, the conditions for which these two approaches are appropriate have not been systematically evaluated.

True linear (e.g., first-order) biodegradation exists only in systems that have no measurable net biomass growth. This may occur when the concentration of substrate, electron acceptor, or nutrient is too low to support net growth, or when the rate of biomass loss (e.g., decay, outflux) is comparable to growth. Breakthrough curves for substrate (contaminant) transport coupled with linear biodegradation exhibit a constant plateau at a concentration that is less than the input concentration (for step input conditions), as illustrated in Fig. 1. This type of transport is referred to herein as steady state transport. Conversely, transport coupled with the nonlinear Monod equation is nonsteady, wherein the effluent substrate concentration first increases to a maximum value, then decreases with time as solute is continually injected into the system (Fig. 1). This time-dependent behavior is due to biomass growth, which results in an increase in substrate demand and a concomitant decrease in effluent concentrations. The conditions for which steady or nonsteady transport behavior is observed have not been examined in detail. Such knowledge would be very useful for enhancing our understanding of

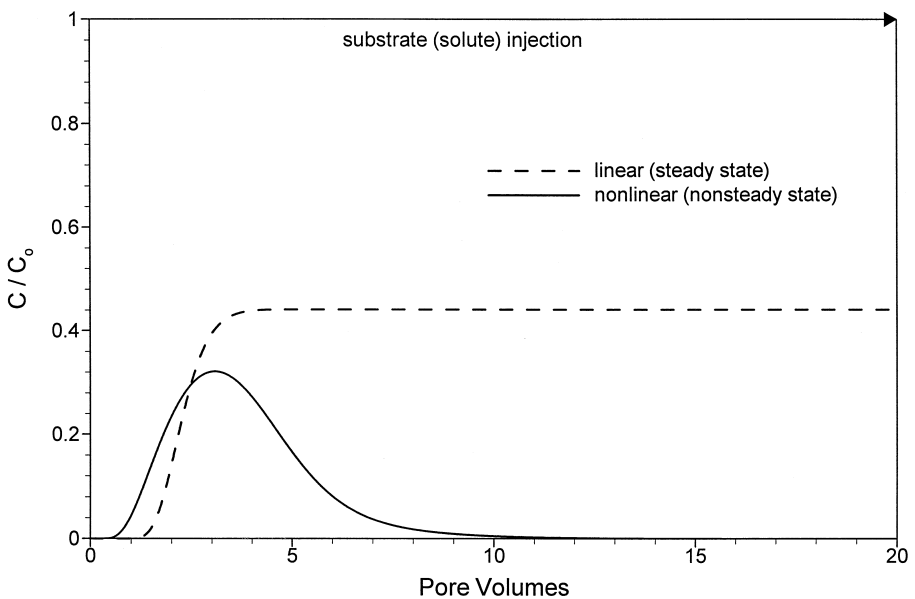

Fig. 1. Typical breakthrough curves for nonlinear and linear biodegradation. Nonlinear case: $t_r = 20$ h, $\mu_m = 0.0958\ h^{-1}$, $M_0 = 5.25$ mg/l, $Y = 0.58$, $C_o = 10$ mg/l, $K_c = 20$ mg/l; linear case: rate coefficient = $0.04\ h^{-1}$, $C_o = 10$ mg/l.

contaminant transport, and for practical applications such as the design and implementation of in situ bioremediation programs.

In a system in which biodegradation is coupled with solute transport, the magnitude and rate of biodegradation is influenced not only by properties of the microbial population and the substrate, but also by hydrodynamic properties (e.g., residence time, dispersivity). The impact of hydrodynamic factors on biodegradation has been studied in laboratory experiments reported by Angley et al. (1992), Estrella et al. (1993), and Kelsey and Alexander (1995). They observed greater biodegradation with lower flow rates or longer path lengths, which was attributed to the longer period of contact (i.e., residence time) between microorganisms and the substrate. Several numerical studies have focused on the effect of selected hydrodynamic factors (e.g., hydraulic conductivity, dispersivity) on biodegradation during transport (Borden and Bedient, 1986; Borden et al., 1986; Celia et al., 1989; MacQuarrie and Sudicky, 1990; MacQuarrie et al., 1990). Other studies have focused on the effect of selected individual biotic or abiotic factors on biodegradation (Sykes et al., 1982; Molz et al., 1990; Widdowson et al., 1988; Chen et al., 1992; Wood et al., 1995; Hu and Brusseau, 1998). Despite this work, the combined factors controlling the behavior of the coupled-process system have not been examined in detail.

The purpose of the research presented herein is to systematically examine the influence of various physical, chemical, and microbial factors on the biodegradation and transport of dissolved contaminants. This is accomplished by nondimensionalizing the governing equations, which produces three characteristic dimensionless parameters. These parameters reflect the influences of biotic and hydraulic properties of the system on biodegradation and transport, which will be illustrated with a series of numerical simulations and 'type-curve' diagrams. The conditions for which steady and nonsteady transport occurs will be examined, as will the impact of biodegradation, with and without biomass growth, on spatial solute distributions and moments.

2. Mathematical framework

2.1. Governing equations

The governing equations for one-dimensional steady state flow, advective and dispersive solute transport, coupled with linear, instantaneous sorption, nonlinear biodegradation, biomass growth and decay, and electron-acceptor availability are:

$$(\theta + \rho K_d)\frac{\partial C}{\partial t} = -q\frac{\partial C}{\partial x} + \theta D_c\frac{\partial^2 C}{\partial x^2} - \frac{\mu_m M\theta}{Y}\left(\frac{C}{K_c + C}\right)\left(\frac{O}{K_o + O}\right) \quad (1)$$

$$\frac{\partial M}{\partial t} = \mu_m M\left(\frac{C}{K_c + C}\right)\left(\frac{O}{K_o + O}\right) - b(M - M_0) \quad (2)$$

$$\theta\frac{\partial O}{\partial t} = -q\frac{\partial O}{\partial x} + \theta D_o\frac{\partial^2 O}{\partial x^2} - \gamma_0\,\mu_m M\theta\left(\frac{C}{K_c + C}\right)\left(\frac{O}{K_o + O}\right) \quad (3)$$

where coefficients and parameters are defined in Appendix A. We use the Monod equation to represent biomass growth and substrate (contaminant) biodegradation. This equation has been widely used for simulating biodegradation in batch systems (Alexander and Scow, 1989), and has been used often for coupling biodegradation and transport (Brusseau et al., 1992). The substrate is assumed to be bioavailable and utilized from solution only, and the biomass is assumed to be immobile. Limitations associated with these and other assumptions will be discussed below.

Eqs. (1)–(3) can be nondimensionalized as follows:

$$R\frac{\partial C^*}{\partial T} = -\frac{\partial C^*}{\partial X} + \frac{1}{P}\frac{\partial^2 C^*}{\partial X^2} - \epsilon_c M^* \left(\frac{C^*}{K_c^* + C^*}\right)\left(\frac{O^*}{K_o^* + O^*}\right) \tag{4}$$

$$\frac{\partial M^*}{\partial T} = \epsilon_m M^* \left(\frac{C^*}{K_c^* + C^*}\right)\left(\frac{O^*}{K_o^* + O^*}\right) - B(M^* - M_0^*) \tag{5}$$

$$\frac{\partial O^*}{\partial T} = -\frac{\partial O^*}{\partial X} + \frac{1}{P}\frac{\partial^2 O^*}{\partial X^2} - \epsilon_o M^* \left(\frac{C^*}{K_c^* + C^*}\right)\left(\frac{O^*}{K_o^* + O^*}\right) \tag{6}$$

by introducing the following dimensionless parameters:

$$X = \frac{X}{L}, \qquad T = \frac{vt}{L}, \qquad P = \frac{vL}{D} \tag{7}$$

$$C^* = \frac{C}{C_o}, \qquad O^* = \frac{O}{O_o}, \qquad M^* = \frac{M}{M_0} \tag{8}$$

$$\epsilon_c = \frac{\mu_m L M_0}{vYC_o} \qquad \epsilon_o = \frac{\gamma_o \mu_m L M_0}{vO_o} \qquad \epsilon_m = \frac{\mu_m L}{v} \qquad B = \frac{bL}{v} \tag{9}$$

$$K_c^* = \frac{K_c}{C_o}, \qquad K_o^* = \frac{K_o}{O_o}, \qquad R = 1 + \frac{\rho}{\theta}K_d \tag{10}$$

The governing equations were solved numerically using the second-order upwind method (Colella, 1990). This method can provide robust results even for small dispersion problems. Appropriate initial and boundary conditions are used for two cases, an input pulse and an existing plume (the latter case is defined below). For the input-pulse case, a flux-type boundary is used for the substrate (and when appropriate the electron acceptor) at $X = 0$. Initial conditions are $C^* = 0$, $S^* = 0$, $O^* = 1$, and $M^* = 1$ within the domain.

2.2. Characteristic controlling parameters

The advantage of using the dimensionless form of the equations is that the number of independent parameters in the system is minimized. As will be shown below, three characteristic controlling parameters, χ, ϵ_m and K_c^*, are introduced through the dimensionless approach, and represent the relative substrate-utilization coefficient, the effective maximum specific growth rate, and the relative half-saturation constant,

respectively. These parameters reflect the combined effects of flow rate, path length, chemical, physical, microbiological properties, and the boundary and initial concentrations of substrate and microorganisms in the system. Below we briefly examine each of these three parameters in isolation.

2.2.1. Effective maximum specific growth rate

In a system with sufficient electron acceptor (e.g., oxygen), the biomass growth rate can be written as:

$$\frac{\partial M^*}{\partial T} = \epsilon_m M^* \frac{C^*}{K_c^* + C^*} \tag{11}$$

where:

$$\epsilon_m = \frac{\mu_m L}{v} = \mu_m t_r \tag{12}$$

and ϵ_m is introduced as the effective maximum specific growth rate for microorganisms, which is a function of residence time t_r and maximum specific growth rate μ_m. The longer the residence time and the larger the maximum specific growth rate, the higher the effective maximum growth rate.

2.2.2. Relative substrate-utilization coefficient

In the absence of electron-acceptor limitation, the substrate or contaminant utilization (biodegradation) rate can be represented by:

$$\frac{\partial C^*}{\partial T} = -\epsilon_c M^* \frac{C^*}{K_c^* + C^*} \tag{13}$$

where

$$\epsilon_c = \frac{\mu_m M_0 L}{Y C_o v} = \mu_m t_r \frac{M_0}{Y C_o} = \epsilon_m \chi \tag{14}$$

and

$$\chi = \frac{M_0}{Y C_o} = \frac{M_0}{\frac{\Delta M}{\Delta C} C_o} = \frac{\frac{\Delta C}{C_o}}{\frac{\Delta M}{M_0}} = \frac{\Delta C^*}{\Delta M^*} \tag{15}$$

with ϵ_c introduced as the apparent biodegradation rate coefficient, and χ defined as the relative substrate-utilization coefficient, which is determined by the initial biomass concentration, substrate boundary input concentration, and the biomass yield coefficient. The higher the effective maximum specific growth rate and the larger the relative substrate-utilization coefficient, the higher the biodegradation rate (i.e., substrate utilization rate). The relative substrate-utilization coefficient can be viewed as the amount of

initial biomass present in the system compared to the supply of substrate. Alternatively, it can be viewed as an inverse nondimensional yield coefficient.

2.2.3. Relative half-saturation constant

Substrate degradation and biomass growth are both controlled by the term $C^*/(K_c^* + C^*)$, where K_c^*, the relative half-saturation constant, is the dimensional half-saturation constant normalized by substrate input concentration. This parameter indicates the affinity of the microbial population to the substrate, relative to the supply of substrate. The larger the relative half-saturation constant, the lower the substrate utilization and biomass growth rates.

3. Results and discussion

3.1. Characteristic controlling parameters

The influence of the characteristic parameters on biodegradation and transport is examined with a series of numerical simulations and sensitivity analyses. As mentioned above, three characteristic parameters, ϵ_m, χ, and K_c^*, control biodegradation during transport. As long as they remain fixed, the biodegradation and transport behavior is the same no matter how the individual factors comprising the characteristic parameters may change. This is illustrated in Fig. 2, wherein are presented the results of three simulations conducted by changing values for μ_m and t_r while keeping ϵ_m fixed at the same value. Breakthrough curves obtained for these cases are identical. This illustrates that the magnitude of biodegradation and the resultant relative substrate concentration distribution are independent of the individual values of maximum specific growth rate μ_m and residence time t_r for a specified ϵ_m. However, the magnitude of biodegradation is dependent on the magnitude of ϵ_m (compare cases 1–3 to case 4). Similar results are obtained for the other two controlling parameters.

The impact of K_c^* on the magnitude of biodegradation during transport is illustrated in Fig. 3A, wherein are presented five simulated curves obtained using a fixed value for C_o and five values for K_c. For these and all simulations discussed in this section, solution containing the contaminant is continuously injected for the length of the simulation. The fraction of contaminant mass degraded (area above the curve) increases as the magnitude of K_c^* decreases. This behavior is associated with the onset of nonsteady transport, or significant increase in substrate utilization, which occurs at earlier pore volumes (or times) as K_c^* decreases. From the Monod equation [$\mu = \mu_m C(K_c + C)^{-1}$], the relative magnitudes of C_o and K_c specify the magnitude of the specific growth rate μ controlling biodegradation. The larger C_o is relative to K_c (i.e., smaller K_c^*), the closer the specific growth rate will be to the maximum, and the sooner the system will attain nonsteady conditions.

The simulation with $K_c^* = 100$ exhibits steady behavior, due to the large difference between K_c and C_o, and minimal mass loss. When C_o is much less than K_c, the amount of substrate available is insufficient to support significant growth, and substrate utilization therefore remains essentially constant. The change in M with time for this

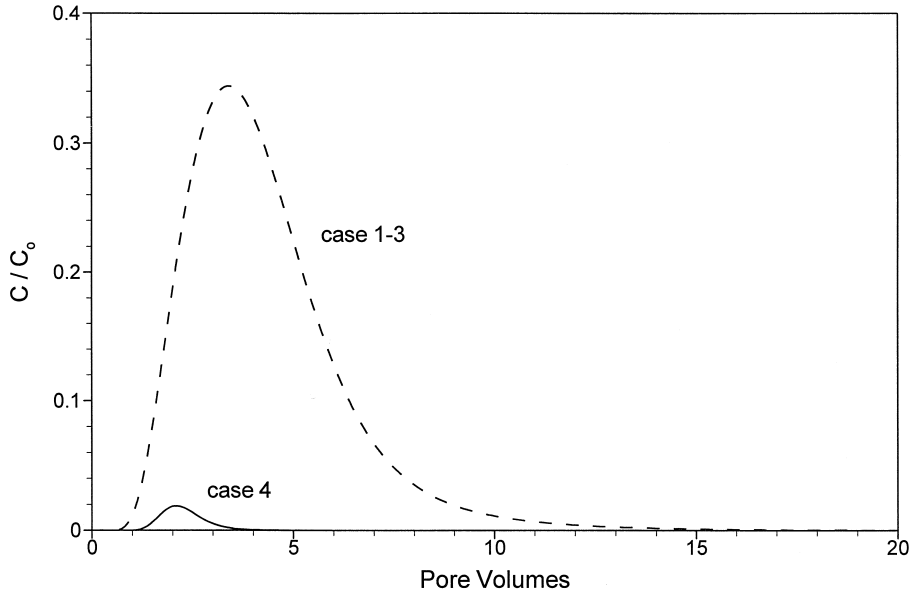

Fig. 2. Influence of μ_m and t_r on magnitude of biodegradation, obtained by fixing ϵ_m and changing μ_m and t_r: case 1: $\mu_m = 0.3832\ h^{-1}$, $t_r = 5$ h, $\epsilon_m = 1.916$; case 2: $\mu_m = 0.0958\ h^{-1}$, $t_r = 20$ h, $\epsilon_m = 1.916$; case 3: $\mu_m = 0.02395\ h^{-1}$, $t_r = 80$ h, $\epsilon_m = 1.916$; case 4: $\mu_m = 0.3832\ h^{-1}$, $t_r = 20$ h, $\epsilon_m = 7.664$; ($M_0 = 5.25$ mg/l, $K_c = 20$ mg/l, $C_o = 10$ mg/l for all cases).

case, compared to the other cases, is shown in Fig. 3B. Clearly, there is little growth when C_o is much less than K_c. Comparison of Fig. 3A and B shows that the onset of nonsteady behavior with respect to contaminant transport corresponds to a significant increase in biomass production.

The impact of χ on the magnitude of contaminant biodegradation is illustrated with a series of simulations presented in Fig. 4. In this series of simulations, all parameter values are kept constant, with the exception of M_0, the initial biomass concentration. The peak height is lower and the onset of nonsteady behavior occurs earlier as the magnitude of χ increases. This results in an increase in the fraction of mass degraded with increasing χ. At larger values of M_0, the demand for substrate is greater, which causes lower peaks. Furthermore, a given relative increase in biomass has a much greater impact on substrate utilization for larger M_0 values because of the differences in absolute numbers. Thus, the impact of biomass growth on increased substrate utilization will occur sooner for larger values of M_0. This is clearly shown in Fig. 4B, which presents the change in biomass concentration during each simulation. The pore volume (or time) at which the maximum rate of growth is attained decreases as χ or M_0 increases.

When χ is sufficiently small, transport will exhibit steady behavior initially, as illustrated in Fig. 4A for the simulation with $\chi = 0.01$. For this case, biomass growth is minimal during the first 30 pore volumes (see Fig. 4C), and as a result there is no significant increase in substrate demand. Thus, the concentration of contaminant in the

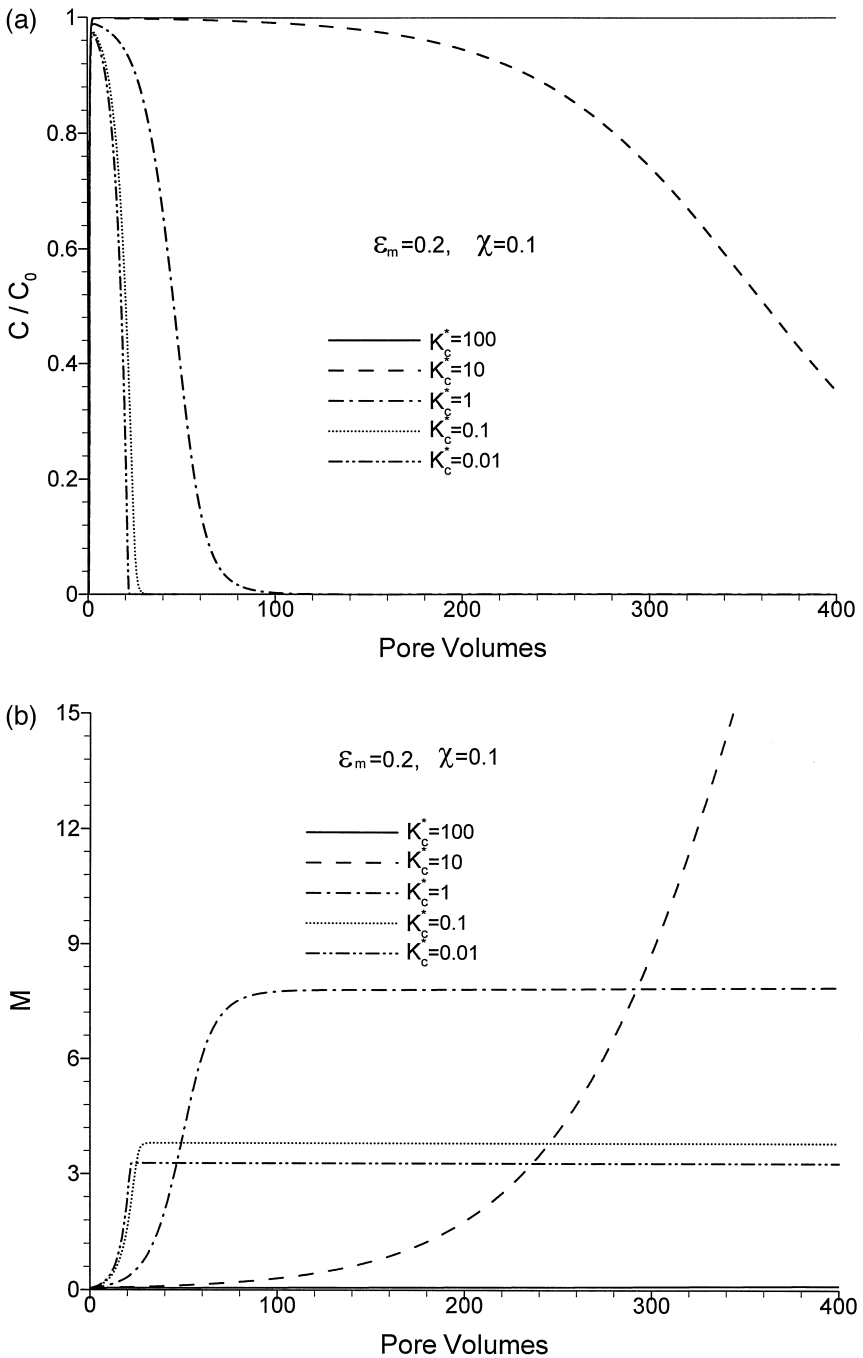

Fig. 3. The influence of K_c^* on biodegradation and transport: (A) contaminant transport; (B) biomass growth at $X \approx L$; $\epsilon_m = 0.2$, $\chi = 0.1$, $C_o = 1$ mg/l. Pore-water velocity is constant for all simulations; thus, pore volumes and real time are equivalent (with $t = 0.087$ T).

effluent remains essentially constant during the first 30 pore volumes. However, after 30 pore volumes, substrate utilization begins to significantly increase as the rate of growth increases, which leads to nonsteady behavior.

When χ is very large, transport may approximate steady behavior as shown in Fig. 4A for the simulation with $\chi = 50$. For such cases where the amount of initial biomass is much greater than the supply of substrate, the total amount of biomass produced in the system is relatively small compared to M_0. Thus, the overall substrate demand will remain relatively constant and transport will exhibit a smaller degree of nonsteady behavior. As shown in Fig. 4D, the relative increase in biomass is greater for smaller values of χ (i.e., smaller M_0). Of course, the absolute increase in biomass is greater for larger χ.

In total, we see that approximately steady state transport behavior may be observed at both smaller and larger magnitudes of χ, while nonsteady transport is expected for intermediate values. For the smaller-magnitude limiting case, the amount of biomass initially present relative to the supply of substrate is too small for growth to have a significant impact on substrate utilization (for 'early' times). However, growth is occurring in such systems, albeit relatively slowly. Conversely, for the larger-magnitude limiting case, the amount of growth relative to the initial biomass is comparatively small due to the limited substrate supply. This analysis clearly shows the impact of the relative amounts of biomass and substrate, as represented by the χ parameter, on the magnitude of biodegradation and the type of transport behavior observed.

In the paragraphs above we examined how the relative magnitudes of C_o and K_c and those of C_o and M_0 influenced biodegradation and transport. We will now examine how the relative magnitudes of the substrate residence time and the characteristic time for growth, as represented by the ϵ_m parameter, influence biodegradation and transport. The impact of ϵ_m on the magnitude of biodegradation during transport is shown in Fig. 5, in which are presented seven simulated curves obtained using a fixed value for μ_m and seven pore-water velocities. The fraction of contaminant mass degraded increases as the magnitude of ϵ_m increases. This behavior is associated with the onset of nonsteady transport, which occurs at earlier pore volumes as ϵ_m increases. No measurable substrate utilization occurs for the case with $\epsilon_m = 0.02$ due to biodegradation being constrained by the very small residence time. In essence, the mean time each contaminant molecule spends in the system is too short for it to be available to the biomass. The magnitude of the C/C_o peak decreases as ϵ_m increases, as would be expected.

The limiting conditions for our system were investigated by examining the range of parameter values associated with the extreme cases of essentially no biodegradation and complete biodegradation, respectively. Complete biodegradation is operationally defined as a sufficient degree of biodegradation such that no breakthrough of contaminant occurs. The effective range for a specific parameter changes as a function of the magnitudes of the other two controlling factors. Thus, there are 12 sets of limiting cases. The results of the analysis are presented in Table 1.

An increase in the magnitude of the effective maximum specific growth rate (ϵ_m) or the relative substrate-utilization coefficient (χ), and a decrease in the relative half-saturation constant (K_c^*) produces a trend toward the limiting case of complete biodegradation. The reverse conditions result in a trend toward no degradation. Inspec-

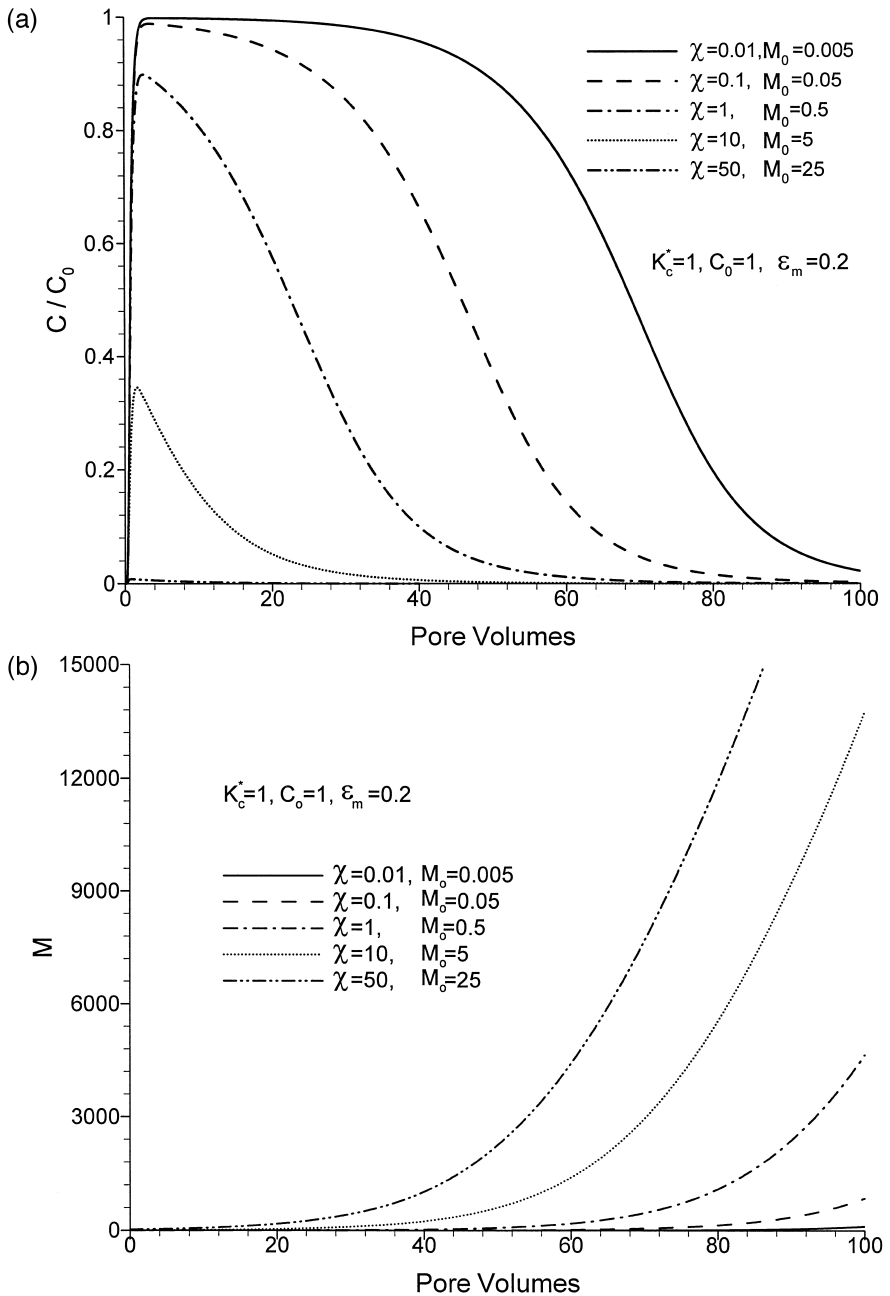

Fig. 4. The influence of χ and initial biomass concentration on biodegradation and transport: (A) contaminant transport; (B) biomass growth at $X \approx 0$ ($x = 0.15$cm); (C) biomass growth at $X \approx L$; (D) relative change in M as a function of x at $T = 100$. [$\epsilon_m = 0.2$, $K_c^* = 1$, $C_o = 1$ mg/l]. Pore-water velocity is constant for all simulations; thus, pore volumes and real time are equivalent (with $t = 0.087$ T).

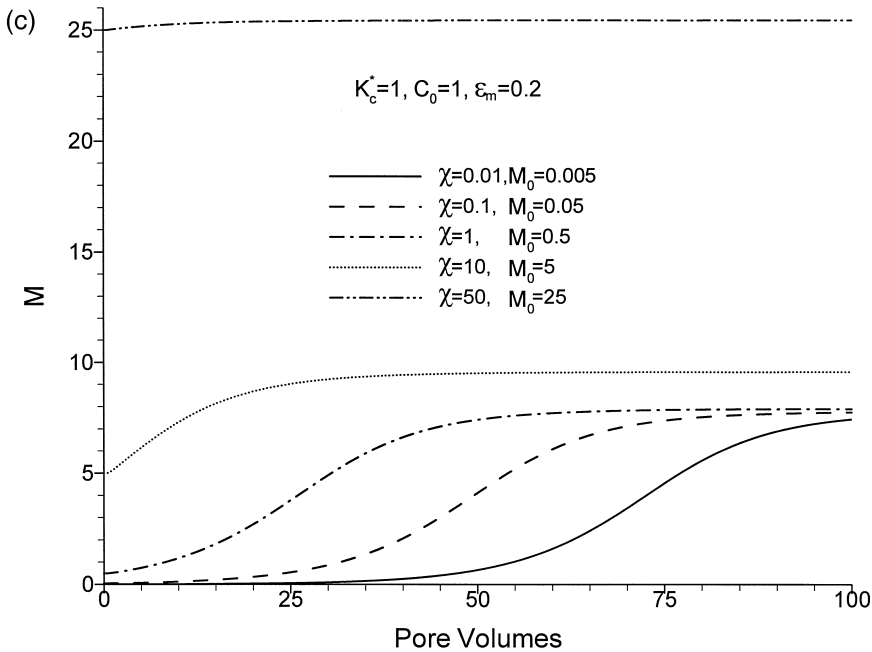

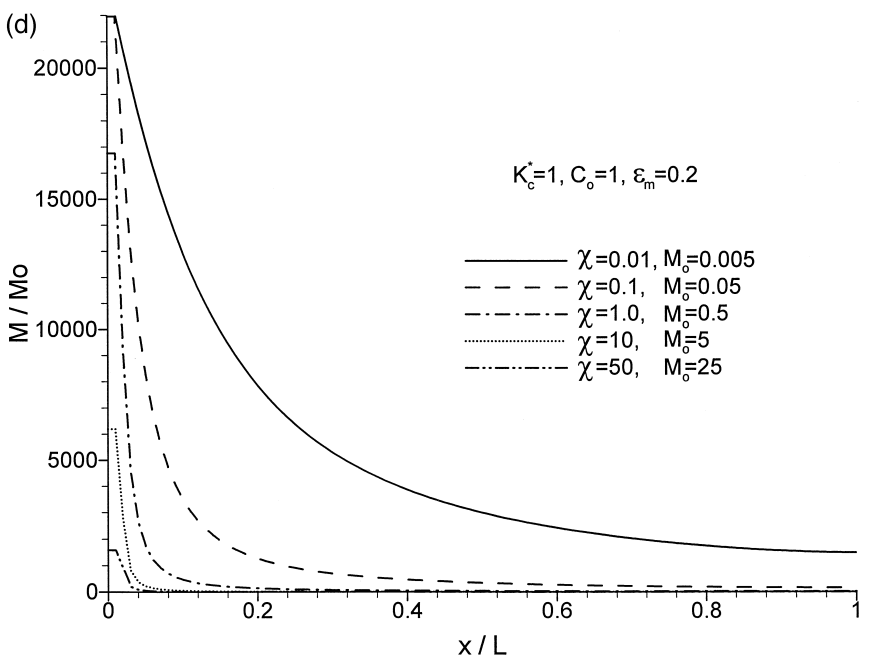

Fig. 4 (continued).

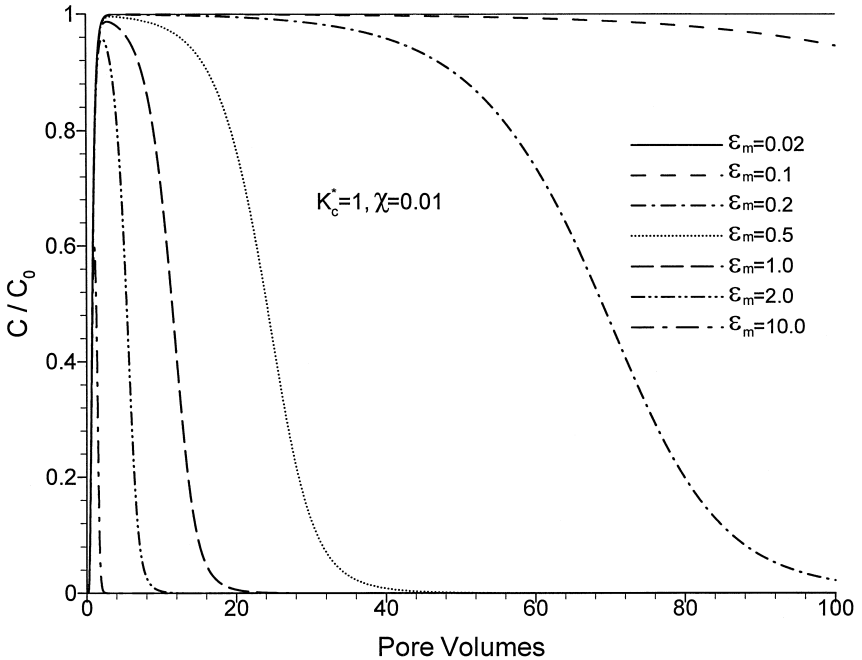

Fig. 5. The influence of ϵ_m on biodegradation and transport; $K_c^* = 1$, $\chi = 0.01$.

tion of Table 1 shows that, for most cases, the effective or operative range of the controlling factors spans either three or four orders of magnitude.

Table 1
Range of parameter values associated with limiting cases

Variable parameter	Fixed parameters[a]	NB[b]	CB[c]
K_c^*	ϵ_L, χ_L	10^6	10^2
K_c^*	ϵ_L, χ_S	10^4	1
K_c^*	ϵ_S, χ_L	100	0.01
K_c^*	ϵ_S, χ_S	1	N.A.
χ	ϵ_L, K_S	N.A.	
χ	ϵ_L, K_L	10^{-10}	10
χ	ϵ_S, K_S	0.01	10
χ	ϵ_S, K_L	1	10^4
ϵ_m	K_S, χ_L	10^{-4}	0.1
ϵ_m	K_S, χ_S	0.01	10
ϵ_m	K_L, χ_L	0.1	100
ϵ_m	K_L, χ_S	1	10^3

[a] L is large magnitude [$\epsilon_m = 100$, $K_c^* = 100$, $\chi = 10$] and S is small magnitude [$\epsilon_m = 0.1$, $K_c^* = 0.01$, $\chi = 0.1$].
[b] NB represents essentially no biodegradation.
[c] CB represents complete biodegradation.

The effective range for K_c^* occurs at very large values when ϵ_m and χ are both large. For example, essentially complete biodegradation occurs when K_c^* is approximately 100 or smaller. Thus, the bacterial population can have a relatively low affinity for the contaminant and still effect complete biodegradation when the growth rate and initial size of the population are large. Conversely, complete biodegradation is not possible when ϵ_m and χ are both small. Of the two intermediate cases, conditions are more favorable for complete biodegradation (and the operative range for K_c^* occurs at larger values) when ϵ_m is large and χ is small. Thus, it is clear that the magnitude of ϵ_m is more critical than that of χ to the effective range of K_c^*.

When conditions are most favorable to biodegradation (i.e., large ϵ_m and small K_c^*), complete biodegradation occurs at essentially any value of χ. Conversely, the magnitude of χ must be relatively large to produce complete degradation when ϵ_m is small and K_c^* is large; i.e., when growth rate and substrate affinity or substrate concentration are small. Of the two intermediate cases, the one most conducive to complete biodegradation is again the case with large ϵ_m.

The case where the effective range for ϵ_m occurs at the smallest magnitudes, and where conditions for complete biodegradation are most favorable, occurs when K_c^* is small and χ is large (high substrate affinity or substrate concentration and large initial biomass). The case least conducive to complete biodegradation occurs when K_c^* is large and χ is small. Of the two intermediate cases, complete biodegradation is more prone to occur when K_c^* is small. Thus, it is clear that the magnitude of K_c^* is more critical than that of χ to the effective range of ϵ_m.

3.2. Steady vs. nonsteady transport behavior

The transport equations can be used to delineate conditions under which linear and nonlinear biodegradation occur. The type of transport behavior observed depends on the magnitudes of the three characteristic parameters, ϵ_m, χ and K_c^* discussed above. A diagram delineating expected transport behavior was constructed using the effective maximum specific growth rate (ϵ_m) for the y axis, the relative half-saturation constant (K_c^*) for the x axis, and the relative substrate-utilization coefficient (χ) as the criterion for each 'type curve'. By fixing χ, and changing ϵ_m and K_c^*, a large number of simulations were conducted to delineate the zones wherein steady and non-steady transport is expected, as shown in Fig. 6.

To use this diagram, the location of the coordinate point corresponding to the specific pair of ϵ_m and K_c^* values associated with a simulation or experiment is compared to the magnitude of the χ parameter (i.e., type curve) associated with that simulation or experiment. If the coordinate point is greater than χ, i.e., if the point is above the type curve, transport should be nonsteady. Conversely, steady state transport is expected when the coordinate point is below the type curve.

From inspection of the diagram, it is clear that, for typical C_o and K_c values, ϵ_m is the primary parameter controlling whether nonsteady or steady transport will occur for a given set of conditions. Larger effective maximum specific growth rates will cause higher biomass growth rates, and more biomass growth, which increases the amount of

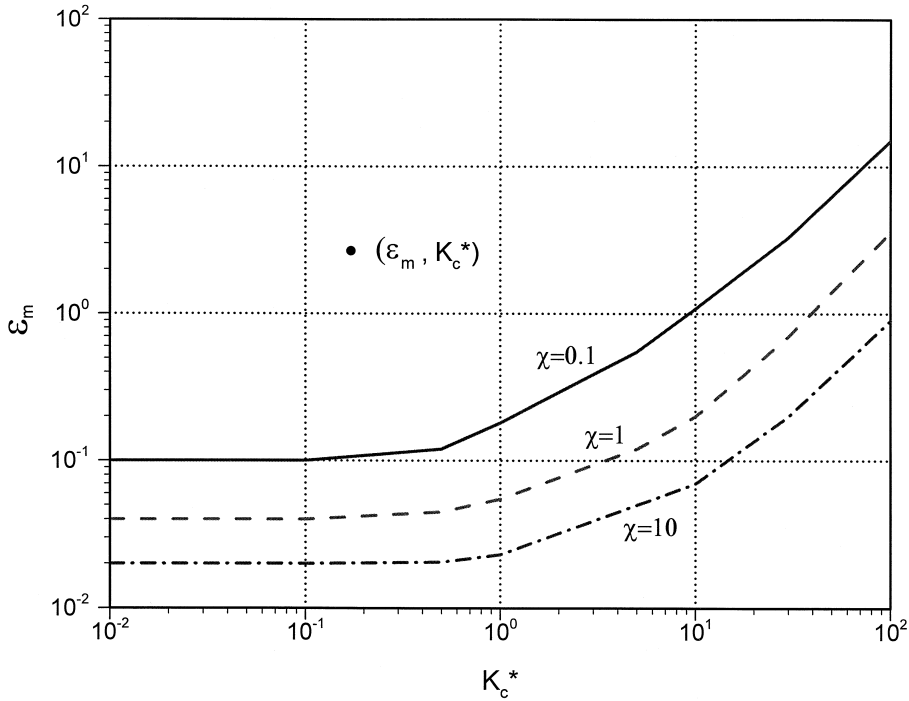

Fig. 6. Type-curve diagram delineating steady (linear biodegradation) and non-steady (nonlinear biodegradation) zones for transport behavior. The zone above a given type curve denotes nonsteady transport and that below steady transport.

substrate degraded. This temporal increase in biomass and associated biodegradation capacity produces a temporal increase in substrate demand, which results in nonsteady transport. Conversely, the minimal growth associated with lower values of ϵ_m results in a relatively constant substrate demand, and corresponding steady state transport.

The ϵ_m parameter consists of the maximum specific growth rate and the hydraulic residence time. Thus, residence time is a critical factor controlling the type of transport exhibited for a given system. Of course, the inherent activity of the microorganisms is also critical. Compared to ϵ_m, the other two parameters have lesser, but still important, effects. For example, different type curves are obtained by using different values for the relative substrate-utilization coefficient, χ. However, a change in χ has a relatively small impact on the position of the type curve.

As indicated in Fig. 6, steady state breakthrough curves will be observed for a small effective maximum growth rate ϵ_m. As K_c^* is increased, the steady state zone increases. In this case, a linear, first-order equation can be used to approximate the nonlinear Monod equation, and the larger the K_c^*, the better the approximation. This is because more substrate is needed to support unit biomass growth for higher K_c^* values (i.e., the system is further away from the maximum specific growth rate), which results in less

biomass production. Therefore, M^* exhibits relatively little change (remains close to 1), which enhances the validity of the first-order approximation:

$$\frac{\partial C^*}{\partial T} = -\frac{M^*\epsilon_c}{K_c^* + C^*}C^* \approx -\frac{\epsilon_c}{K_c^*}C^* = -\epsilon_1 C^* \tag{16}$$

where ϵ_1 is the nondimensional first-order degradation rate coefficient.

It is important to note that to maintain practicality with a focus on field applications, the type-curve diagram is based on relatively short-term behavior observed after the introduction or perturbation of a substrate pulse. Specifically, we have focused on the behavior exhibited during the first 20–25 pore volumes after introduction of a contaminant pulse, or after a perturbation to an existing contaminant plume. Thus, it must be stressed that the designation of steady state transport obtained from use of the type curve may often apply only for the initial portion of the event. For example, the coordinate points for three of the cases presented in Fig. 5 ($\epsilon_m = 0.02$, 0.1, 0.2) fall below the type-curve line of $\chi = 0.01$. Thus, steady state behavior is expected for these three cases. Inspection of Fig. 5 shows that such behavior is observed for the three cases, but that it lasts only for the first 20 or 50 pore volumes for the $\epsilon_m = 0.2$ and 0.1 cases, respectively. Similar behavior is illustrated in Fig. 4, where the case with $\chi = 0.01$ is expected to exhibit steady state behavior, which it does for the first 20 pore volumes. In general, while many systems may have the potential to exhibit nonsteady transport, it is likely that it may often not be observed due to practical constraints. This will be governed by the relative magnitudes of the time required for the onset of nonsteady behavior and the time scale of interest.

3.3. Growth constraints

In the analyses presented above, the system was simplified to enhance our examination of the coupling between substrate supply, microbial growth, substrate demand, residence time, and resultant transport behavior. This included assumptions that the substrate is readily available to the biomass, that nutrient and electron acceptor concentrations are not limiting, that biodegradation proceeds immediately upon uptake (no lag effects), that biomass decay is negligible, and that the biomass is immobile. Of course one or more of these assumptions may often be invalid, especially under field conditions, as shown by numerous studies. In such cases, the magnitude and rate of biodegradation, and the associated transport behavior, may be constrained by any one of these factors. This will be illustrated by examining the impact of electron-acceptor limitation and biomass decay on biodegradation and transport.

The concentration of the electron acceptor would be another factor controlling the rate of biodegradation for a system wherein the electron acceptor is limited. The half-saturation constant of the electron acceptor, which indicates the affinity of the microorganisms to the electron acceptor, would be an additional controlling parameter if boundary and initial electron-acceptor concentrations are fixed. The higher the K_o, the greater the amount of electron-acceptor required for biomass growth, and the lower the biodegradation rate. Thus, the type curve would move upward and result in a smaller area for the nonsteady transport zone (see Fig. 7). The magnitude of the impact of

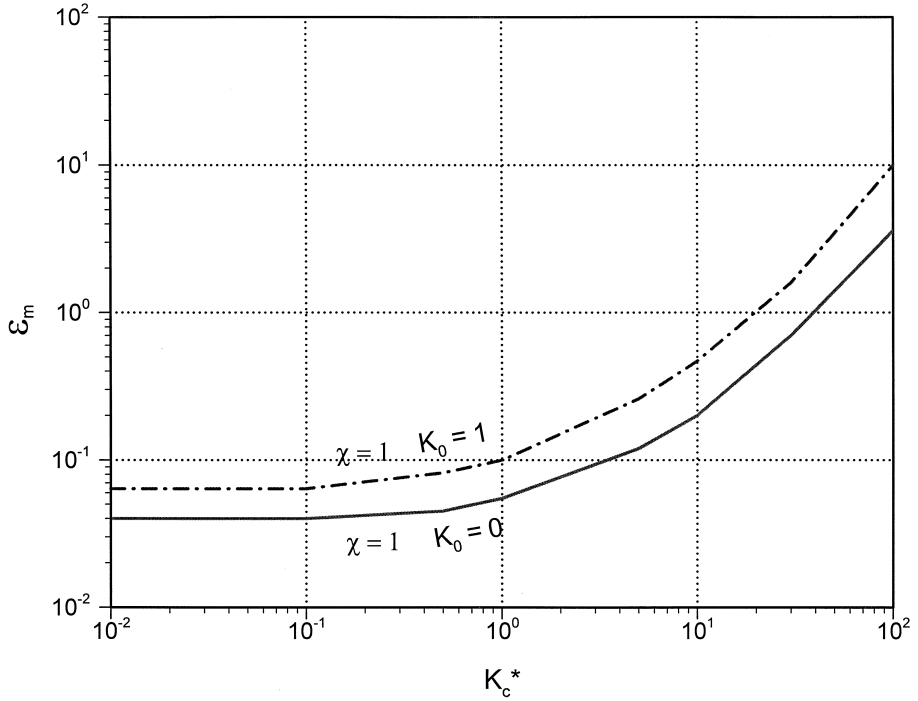

Fig. 7. The influence of electron-acceptor limitation on transport behavior as illustrated with the type-curve diagram.

electron-acceptor limitation on the system depends on the magnitude of ϵ_m. The impact is relatively small for relatively small growth rates, for which the demand for the electron acceptor is relatively small. At higher maximum growth rates, the demand for the electron acceptor is greater and the impact would be more significant. The impact of nutrient limitations would be similar to those associated with electron-acceptor limitations.

As mentioned above, the previous analyses were conducted with an assumption that biomass decay was negligible. This condition may often be valid during the times when a substrate pulse is first introduced to the system. However, at some point, the impact of microbial decay may become significant, due to several potential reasons. Biomass decay obviously mediates the net amount of growth occurring in the system, and thus will influence transport behavior. This is illustrated with the series of simulations presented in Fig. 8.

Biomass decay has minimal impact on biodegradation and transport when decay is much slower than growth, as seen by comparing the simulation obtained with $B = 0$ to the one obtained with $B = 0.002$. For the latter simulation, the magnitude of the nondimensional decay rate coefficient, B, is 100 times smaller than the nondimensional biomass growth rate coefficient, ϵ_m. When B is one-tenth of ϵ_m, biomass decay has a measurable impact on the magnitude of biodegradation, but transport remains nonsteady.

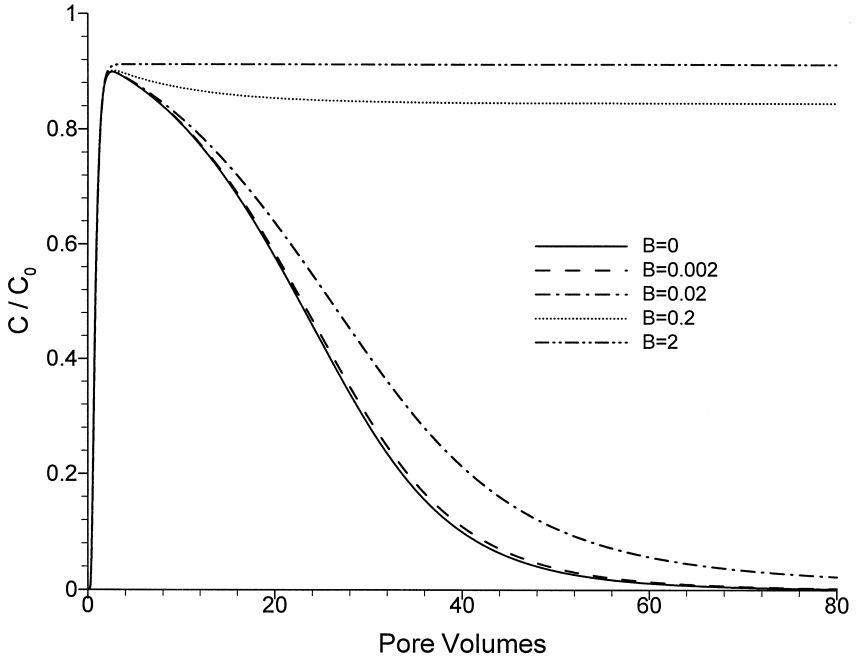

Fig. 8. The influence of biomass decay on biodegradation and transport; $\epsilon_m = 0.2$, $K_c^* = 1$, $\chi = 1$. Pore-water velocity is constant for all simulations; thus, pore volumes and real time are equivalent (with $t = 0.087$ T).

However, when the rate of biomass decay is equal to or greater than the rate of growth (i.e., when $B \geq \epsilon_m$), steady state transport is observed. The effects illustrated with Fig. 8 may also be induced by biomass transport when it causes elution of cells from the system, which acts to moderate net biomass growth and can be represented in a simple manner as another form of biomass loss (i.e., decay).

3.4. Impact of biodegradation on spatial contaminant distributions and moments

The impact of the controlling factors on biodegradation and transport was investigated above by focusing on temporal concentration distributions (i.e., breakthrough curves). However, the influence of various factors on solute transport is often evaluated by examining their impact on spatial distributions. The impact of linear and nonlinear biodegradation on spatial solute distribution and moments will be examined in this section for two cases, an existing plume and an input pulse. The existing-plume case represents systems with resident contamination, such as those found at hazardous waste sites. The input-pulse case represents conditions such as those associated with a tracer study. Three sets of simulations are conducted for each case: (1) no biodegradation, (2) linear (first-order) biodegradation, and (3) nonlinear (Monod) biodegradation. Sorption is linear and instantaneous for all simulations. The analysis is conducted using the parameter values listed in Table 2.

Table 2
Parameter values for moment analysis simulations

Parameter	Value
Porosity	0.3
Soil bulk density	1.5 g/cm^3
Pore-water velocity	0.1 m/d
Dispersion coefficient	0.000625 m
Reference length	0.3 m
Sorption coefficient	0.43 ml/g
Maximum specific growth rate	0.0958 d^{-1}
Yield coefficient	0.8
Substrate half-saturation constant	3 mg/l
Oxygen half-saturation constant	1 mg/l
Biomass decay coefficient	0.0025 d^{-1}
Initial/boundary C	1 mg/l
Initial/boundary O	No limitation
Initial M	1.25 mg/l
Input pulse	30 pore volumes

For the initial-plume case, the plume occupies the 10 relative length units nearest the upgradient boundary. Inside the plume, the initial relative concentrations of substrate and biomass are both 1. Outside the plume, the initial relative concentrations of substrate and biomass are 0 and 1, respectively. The boundary conditions are given by:

$$C^* - \frac{1}{P}\left(\frac{\partial C^*}{\partial X}\right)_{X=0} = 0 \tag{17}$$

$$\left(\frac{\partial C^*}{\partial X}\right)_{X=L} = 0 \tag{18}$$

The pulse interval for the input-pulse case is 30 dimensionless time units, which generates a plume equivalent to that used for the existing-plume case. The initial relative concentrations of substrate and biomass are 0 and 1, respectively, in the domain. The upgradient boundary is given by:

$$C^* - \frac{1}{P}\left(\frac{\partial C^*}{\partial X}\right)_{X-0} = C_o^* \tag{19}$$

where $C_o^* = 1$ for $O < T \leq 30$, and $C_o^* = 0$ for $T > 30$. The downgradient boundary condition is given by Eq. (18).

3.4.1. Existing-plume case

The spatial distributions of contaminant for linear biodegradation exhibit uniform peak concentrations (i.e., constant plateau), as shown in Fig. 9A. The magnitude of the plateau decreases with time due to continued degradation. However, the rate of reduction decreases as the concentration (driving force) decreases. Conversely, the spatial distributions for nonlinear biodegradation exhibit a nonuniform plateau (Fig. 9B). This results from the spatial variability of biomass growth, which is greater in the

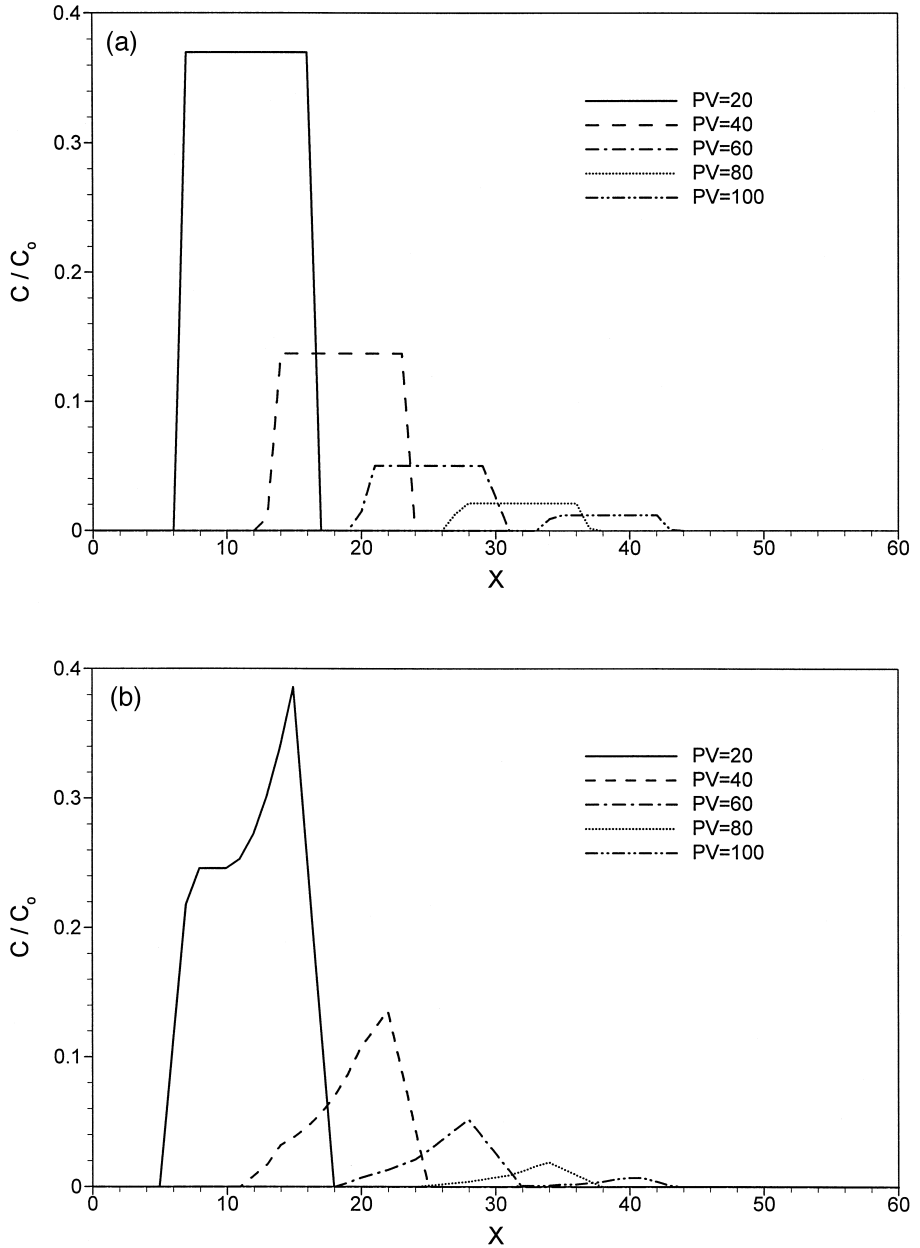

Fig. 9. Spatial contaminant distribution for transport with biodegradation, existing-plume case: (A) linear biodegradation; (B) nonlinear biodegradation.

upgradient region because it has been exposed to substrate the longest. The larger biomass concentration exerts a greater demand on substrate, which results in reduced substrate concentrations in that region.

Linear biodegradation has no effect on the rate of plume displacement (first moment) or the plume shape (skewness) for the conditions of the simulation (minimal dispersion), as shown in Fig. 10. For an existing-plume case, each contaminant molecule has been in

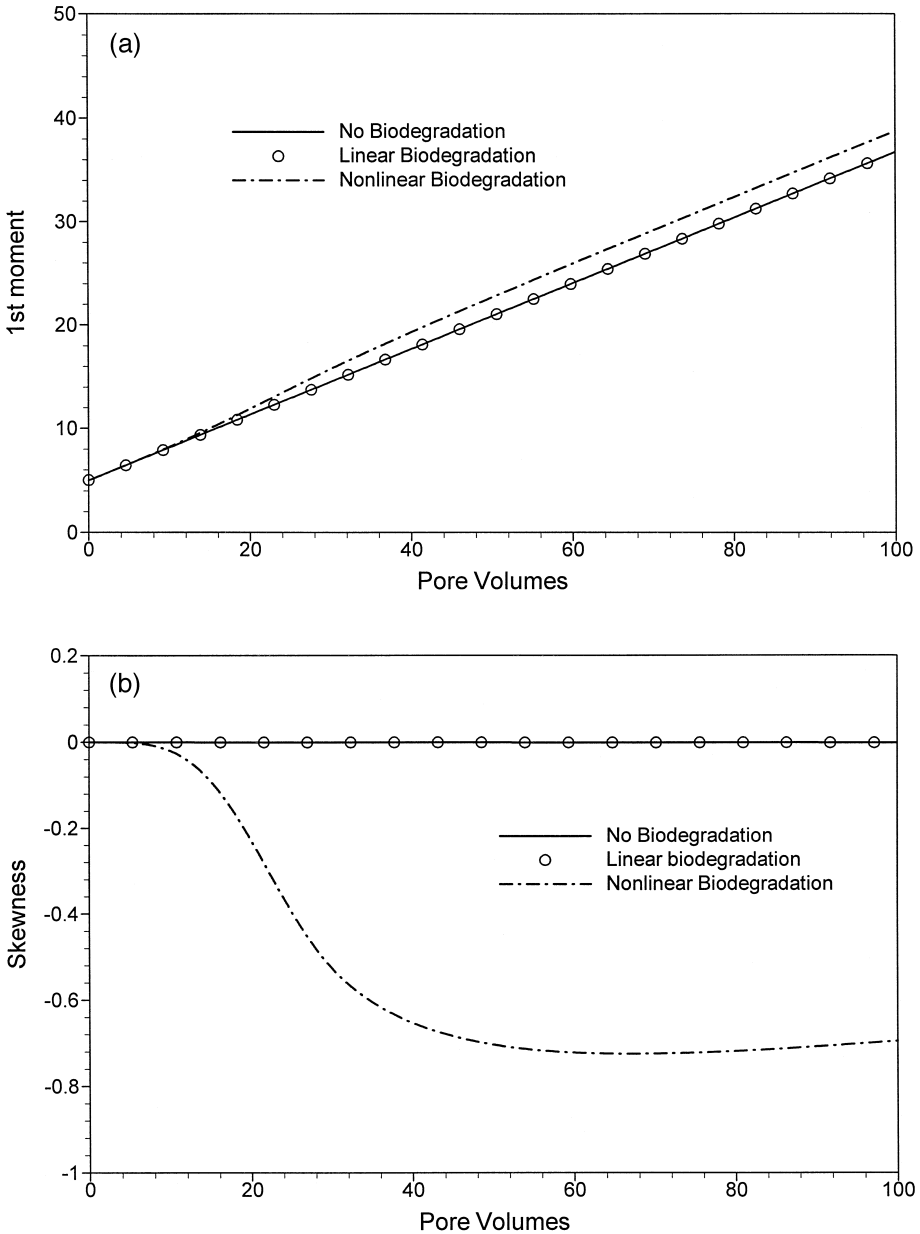

Fig. 10. Spatial moments for transport with no, linear and nonlinear biodegradation, existing-plume case: (A) first moment; (B) third moment (skewness).

the system the same amount of time, and will therefore experience the same degree of degradation. Thus, the plume is degraded uniformly, which results in no impact on the spatial moments. Conversely, the spatial variability of degradation for the nonlinear

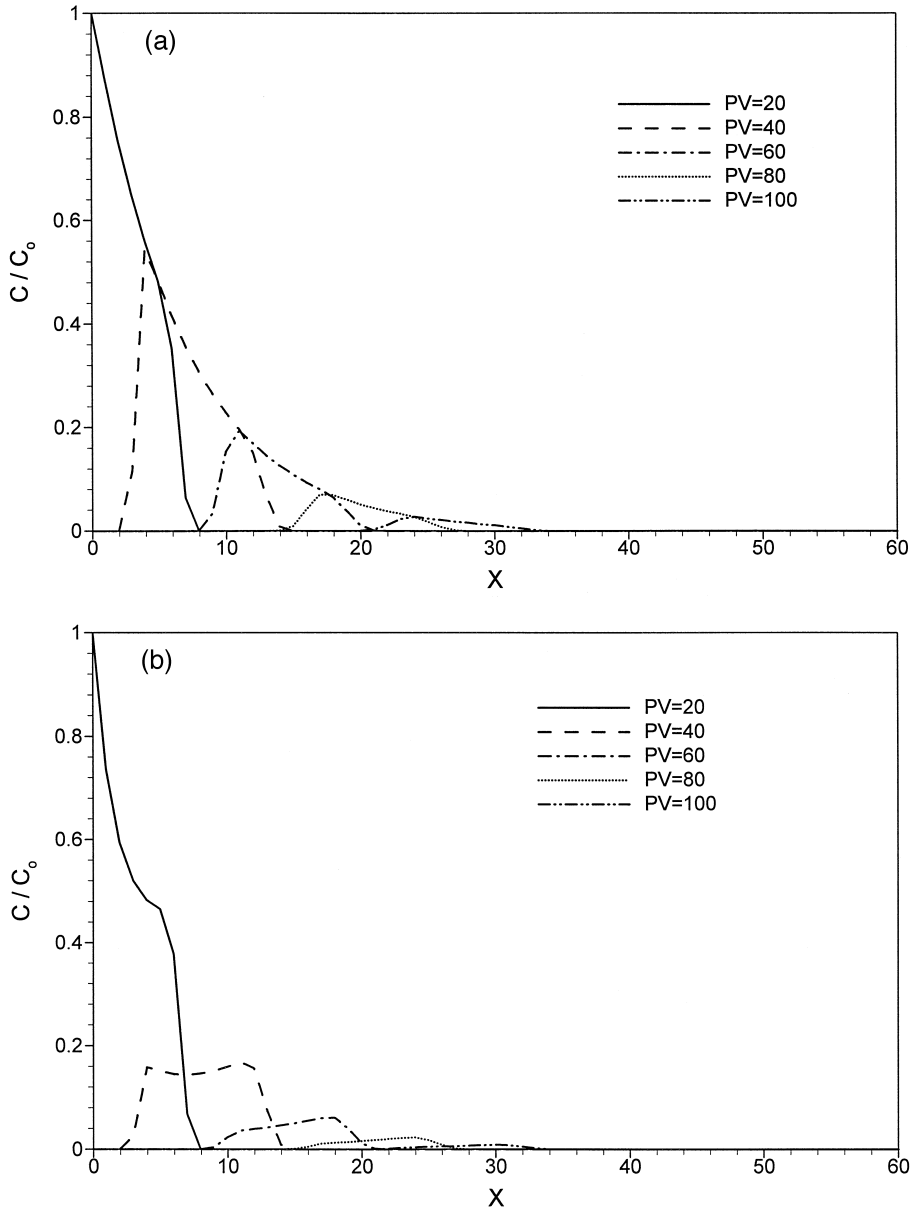

Fig. 11. Spatial contaminant distribution for transport with biodegradation, input-pulse case: (A) linear biodegradation; (B) nonlinear biodegradation.

biodegradation case causes the center of mass of the plume to shift downgradient, which results in an increased first moment (Fig. 10A). It is important to note that this increase in the rate of plume displacement does not mean that the individual contaminant molecules are traveling faster than for the linear-biodegradation or no-biodegradation cases. The higher rate of degradation in the upgradient region reduces the spreading of the plume (not shown), and creates a negative skewness (Fig. 10B).

3.4.2. Input-pulse case

For the input-pulse case, the spatial solute distribution exhibits a nonuniform plateau when biodegradation is linear (Fig. 11A), in contrast to the existing-plume case (Fig. 9A). The nonuniform contaminant distribution is caused by the fact that residence time varies with position within the pulse. The downgradient portions of the pulse have been in the system longer, and thus have experienced more degradation. Conversely, as discussed above, the residence time is uniform for the existing-plume case, which results in uniform degradation and no resultant impact on the spatial moments. In contrast, the first and second moments are reduced (not shown) and positive skewness is exhibited (Fig. 12) for the input-pulse case because the center of mass is shifted upgradient due to the variable residence times and associated magnitudes of degradation.

Variable behavior is observed for the input-pulse case with nonlinear biodegradation (Fig. 11B). At early times, the nonuniform solute distribution is skewed with higher concentrations upgradient for the reason discussed for the linear-biodegradation, input-pulse case (nonuniform residence times). However, at later times, the distribution shifts

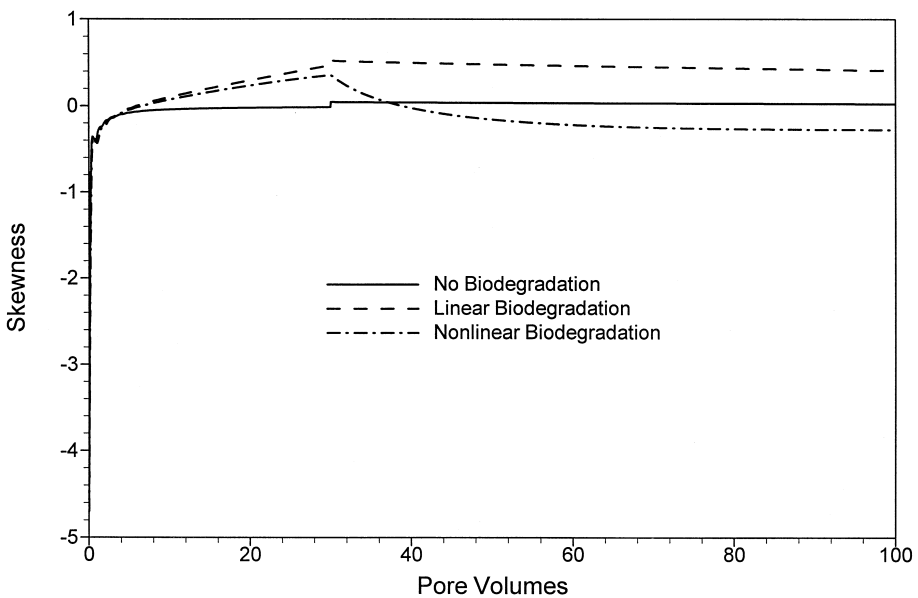

Fig. 12. Third spatial moments (plume skewness) for transport with no, linear and nonlinear biodegradation, input-pulse case.

to where the highest concentrations are on the downgradient side of the pulse as preferential growth reduces concentrations in the upgradient region, similarly to the nonlinear, existing-plume case. This phenomenon can be observed by examining the spatial skewness for the input-pulse case, which changes from positive to negative (Fig. 12), whereas the skewness for the existing-plume case remains negative (Fig. 10B). This change in behavior also affects the first moment, where it is first smaller than and then larger than the case with no biodegradation. These results illustrate the complex impact of boundary conditions, residence time, and biomass growth dynamics on transport.

4. Summary

We have shown the influence of the three controlling factors on transport with nonlinear biodegradation. Overall, the magnitude of biodegradation is the highest for the largest effective maximum specific growth rate ϵ_m and lowest relative half-saturation constant K_c^*. In this case, breakthrough curves are non-steady and may show complete degradation (i.e., zero substrate effluent concentration after a certain pore volume). With the decrease of ϵ_m or the increase of K_c^*, the magnitude of biodegradation decreases and breakthrough curves show incomplete, non-steady, degradation. For all combinations of K_c^* and ϵ_m values below a given type curve, the magnitude of biodegradation is relatively small, and steady state breakthrough curves are observed initially. The impact of biodegradation on the spatial moments was shown to depend on boundary conditions, residence time, and biomass growth dynamics.

Acknowledgements

This research was supported by grants provided by the National Institute of Environmental Health Sciences Superfund Basic Sciences Research Program and the US Environmental Protection Agency Joint Bioremediation Program.

Appendix A. Nomenclature

b	first-order biomass decay coefficient [1/T]
B	effective biomass decay rate coefficient [bL/v]
C	substrate (contaminant) concentration [M/L^3]
C^*	relative substrate concentration [C/C$_o$]
C_o	substrate boundary input concentration [M/L^3]
D_c	substrate hydrodynamic dispersion coefficient [L^2/T]
D_o	electron acceptor hydrodynamic dispersion coefficient [L^2/T]
F	fraction of sorbent for which sorption is instantaneous
k_2	first-order reverse sorption rate coefficient [1/T]
K_d	equilibrium sorption coefficient [L^3/M]
K_c	half-saturation constant for substrate [M/L^3]

K_c^*	relative half-saturation constant for substrate $[K_c/C_o]$
K_o	half-saturation constant for electron acceptor $[M/L^3]$
K_o^*	relative half-saturation constant for electron acceptor $[K_o/O_0]$
L	characteristic (system) length [L]
M	biomass concentration $[M/L^3]$
M_0	initial biomass concentration $[M/L^3]$
O	electron-acceptor concentration $[M/L^3]$
O^*	relative electron-acceptor concentration $[O/O_0]$
P	Peclet number $[vL/D]$
q	Darcy velocity $[L/T]$
R	Retardation factor $[1 + \rho K_d/\theta]$
S	Sorbed-phase concentration of substrate $[M/M]$
S_0	initial sorbed-phase concentration $[M/M]$
S^*	relative sorbed-phase concentration $[S/S_0]$
t	time [T]
t_r	residence time $[L/v]$
T	pore volume or nondimensional time $[tv/L]$
v	pore-water velocity $[L/T]$
x	distance [L]
X	relative distance $[x/L]$
Y	yield coefficient for microorganisms $[M/M]$ (biomass produced/mass of substrate degraded)
ϵ_c	effective substrate degradation rate coefficient $[\mu_m L M_0 (vYC_0)^{-1}]$
ϵ_1	nondimensional first-order biodegradation rate coefficient $[\mu_m M_0 L (YK_c v)^{-1}]$
ϵ_m	effective biomass growth rate coefficient $[\mu_m L/v]$
ϵ_o	effective electron acceptor consumption rate coefficient $[\gamma_0 \mu_m M_0 L (O_0 v)^{-1}]$
ρ	bulk density of porous medium $[M/L^3]$
μ	specific growth rate of microorganism $[1/T]$
μ_m	maximum specific growth rate of microorganism $[1/T]$
γ_0	stoichiometric coefficient equal to the mass of electron acceptor utilized by microorganisms per unit mass of 'substrate' degraded
θ	fractional volumetric water content
χ	relative substrate utilization coefficient $[M_0/YC_0]$

References

Alexander, M., Scow, K.M., 1989. Kinetics of biodegradation in soil. In: Reactions and Movement of Organic Chemicals in Soils, Chap. 10, Special Pub. No. 22, Soil Science Soc. Am., Madison, WI.

Angley, J.T., Brusseau, M.L., Miller, W.L., Delfino, J.J., 1992. Nonequilibrium sorption and aerobic biodegradation of dissolved alkylbenzenes during transport in aquifer material: column experiments and evaluation of a coupled-process model. Environ. Sci. Technol. 26, 1404–1410.

Borden, R.C., Bedient, P.B., 1986. Transport of dissolved hydrocarbons influenced by oxygen-limited biodegradation: 1. Theoretical development. Water Resour. Res. 22, 1973–1982.

Borden, R.C., Bedient, P.B., Lee, M.D., Ward, C.H., Wilson, J.T., 1986. Transport of dissolved hydrocarbons influenced by oxygen-limited biodegradation: 2. Field application. Water Resour. Res. 22, 1983–1990.

Brusseau, M.L., Rao, P.S.C., Bellin, C.A., 1992. Modeling coupled processes in porous media: sorption, transformation and transport of organic solutes. In: Wagenet, J., Baveye, P., Stewart, B.A. (Eds.), Interacting Processes in Soil Science. Advances in Soil Science, Lewis Pub., Ann Arbor, MI, pp. 147–184.

Celia, M.A., Kindred, J.S., Herrera, I., 1989. Contaminant transport and biodegradation: I. A numerical model for reactive transport in porous media. Water Resour. Res. 25, 1141–1148.

Chen, Y.M., Abriola, L.M., Alvarez, P.J.J., Anid, P.J., Vogel, T.M., 1992. Modeling transport and biodegradation of benzene and toluene in sandy aquifer material: comparisons with experimental measurements. Water Resour. Res. 28 (7), 1833–1847.

Colella, P., 1990. Multidimensional upwind methods for hyperbolic conservation laws. J. Comp. Phys. 87, 171–180.

Estrella, M.R., Brusseau, M.L., Maier, R.S., Pepper, I.L., Wierenga, P.J., Miller, R.M., 1993. Biodegradation, sorption and transport of 2,4-dichlorophenoxyacetic acid in saturated and unsaturated soils. Appl. Environ. Micro. 59 (12), 4266–4273.

Hu, M.Q., Brusseau, M.L., 1998. Coupled effects of nonlinear, rate-limited sorption and biodegradation on transport of 2,4-dichlorophenoxyacetic acid in soil. Environ. Toxicol. Chem. 17 (9), 1673–1680.

Kelsey, J.W., Alexander, M., 1995. Effect of flow rate and path length on *p*-nitrophenol biodegradation during transport in soil. Soil Sci. Soc. Am. J. 59, 113–117.

MacQuarrie, K.T.B., Sudicky, E.A., 1990. Simulation of biodegradable organic contaminants in groundwater: 2. Plume behavior in uniform and random flow fields. Water Resour. Res. 26, 223–239.

MacQuarrie, K.T.B., Sudicky, E.A., Frind, E.O., 1990. Simulation of biodegradable organic contaminants in groundwater: I. Numerical formulation in principle directions. Water Resour. Res. 26, 207–222.

Molz, F.J., Widdowson, M.A., Benefield, L.D., 1990. Simulation of microbial growth dynamics coupled to nutrient and oxygen transport in porous media. Water Resour. Res. 22 (8), 1207–1216.

Sykes, J.F., Soyupak, S., Farquhar, G.J., 1982. Modeling of leachate organic migration and attenuation in groundwaters below sanitary landfills. Water Resour. Res. 18 (1), 135–145.

Widdowson, M.A., Molz, F.J., Benefield, L.D., 1988. A numerical transport model for oxygen- and nitrate-based respiration linked to substrate and nutrient availability in porous media. Water Resour. Res. 24 (9), 1553–1565.

Wood, B.D., Ginn, T.R., Dawson, C.N., 1995. Water Resour. Res. 31, 553–563.